Multiobjective optimization of Vortex Generators for heat transfer enhancement in turbulent flows

H. Karkaba, T. Dbouk, C. Habchi, Serge Russeil, Thierry Lemenand, D. Bougeard

International Journal of Thermofluids 22 (2024) 100633

Contents lists available at ScienceDirect

International Journal of Thermofluids

journal homepage: www.elsevier.com/locate/ijtf

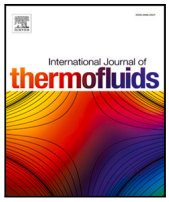

Multiobjective optimization of Vortex Generators for heat transfer enhancement in turbulent flows

H. Karkaba [a,*], T. Dbouk [b], C. Habchi [c,d], S. Russeil [a], T. Lemenand [e], D. Bougeard [a]

[a] IMT Nord Europe, Institut Mines-Télécom, Univ. Lille, Centre for Energy and Environment, F-59000 Lille, France
[b] CORIA, UMR 6614, CNRS, Normandy Univ., UNIROUEN, 76000 Rouen, France
[c] Multiphysics Interaction Lab (MiLab), Los Angeles, CA 90703, USA
[d] IMSIA UMR CNRS-EDF-CEA-ENSTA 9219, Institut Polytechnique de Paris, 91120 Palaiseau, France
[e] LARIS EA 7315, Polytech Angers, Université d'Angers, 49000, Angers, France

ARTICLE INFO

Keywords:
Multi-functional heat exchangers
Vortex Generator
Turbulence
Shape optimization
Forced convection

ABSTRACT

Convective heat transfer can be enhanced by streamwise vortices and coherent flow structures produced downstream Vortex Generators (VGs). The thermal performance depends on the VG shape which controls the intensity and topology of the vortices. Thus, VG shape optimization is a major challenge in designing sustainable and efficient heat exchangers. In the present study, a multi-objective optimization is performed through large space exploration design to find optimal VG shapes that adapt to different flow regimes. Simulations are carried out in parallel plate turbulent flow for three different Reynolds numbers; Re_1 = 4600, Re_2 = 9920, and Re_3 = 30050. The present numerical results are first validated against numerical and experimental data from the open literature. Then, and for the first time, seven design parameters are investigated, based on VG shape dimensions. The new optimized VG show a thermal enhancement factor between 11 and 35%, relative to a smooth channel case, and between 3 and 14%, relative to different VG shapes from the recent open literature. The present results are analyzed in details by focusing on the physics of the flow structure and its correlation to the convective heat transfer enhancement using local criteria for flow visualization and vortex intensity quantification.

1. Introduction

Multi-functional heat exchangers/reactors (MHER) are main components of various devices that are used in many industrial and renewable energy applications. Increasing their performances through heat transfer enhancement and pressure drop reduction is important to energy savings. Different techniques for heat transfer enhancement are found that can be named as active, passive, and dynamic. The active techniques require external power such vibration, electromagnetic field, jet impingement techniques. Meanwhile, the passive techniques do not require any external forces and they mainly use surface deformation methods such as vortex generators (VGs) [1–6]. Dynamic techniques employ dynamic and elastic surfaces such as flexible VGs [7,8].

Wang et al. [9] conducted a comprehensive review on heat transfer enhancement technologies classified as passive and active techniques with variety of applications. In addition, they introduced a hybridization of two or more techniques that provide a novel heat transfer enhancement methods. Different usage applications of these techniques are presented as heat exchangers, reactors, mini or micro-channels, etc. Brodnianska et al. [10] studied the heat transfer enhancement in a novel wavy shaped heat exchanger channel via inserting cylindrical vortex generators. The study performed with the variation of the flow rates by means the Reynolds number and compared to smooth channels. In addition correlations were developed for this type of technique which can be helpful when designing and analyzing such configuration. Such correlations can be used to develop dynamic models for specific systems as done by Karkaba et al. [11] for a solar applications system improvement that is achieved by the use of VG's. Chamoli et al. [12] studied numerically the thermal improvement in a solar air heater by using various shapes of winglet vortex generators. It was found that the heat enhancement factor (TEF) increased in a range of 1.72 to 2.2 with an angle of attack equals to 30% and zero tip edge ratio. VG technique can also be used in improving the performance of battery thermal management systems for electrical vehicles. Ye et al. [13] performed multi-variable analysis of vortex generator-aided heat transfer enhancement for battery cooling. Results showed a 56.4% reduction in temperature difference (2.66 K) and a 12.1% decrease in the maximum temperature (2.75 K).

* Corresponding author.
E-mail address: hassan.karkaba3@gmail.com (H. Karkaba).

https://doi.org/10.1016/j.ijft.2024.100633
Received 9 January 2024; Received in revised form 15 March 2024; Accepted 16 March 2024
Available online 19 March 2024

Nomenclature

Principle notation

A	Area (m^2)
C_p	Specific heat ($Jkg^{-1}K^{-1}$)
d	Distance between VGs (m)
D_h	Hydraulic diameter (m)
f	Friction factor (–)
F	Pumping power factor (–)
h	Heat transfer coefficient, height of the VG ($Wm^{-2}K^{-1}$, m)
H	Height of the channel (m)
j	Stream-wise vorticity flux (–)
J	Heat transfer performance factor (–)
k	Turbulent kinetic energy (Jkg^{-1})
k_f	Fluid thermal conductivity ($Wm^{-1}K^{-1}$)
l	Length of the VG (m)
L	Length of the channel (m)
$\dot{m}$	mass flow rate (kgs^{-1})
Nu	Nusselt number (-)
p	Pressure (Pa)
Pr	Prandtl number (-)
q''	Boundary heat flux (Wm^{-2})
Re	Reynolds number (-)
S	Surface area (m^2)
SL	Shape length of the VG (m)
T	Temperature (K)
T_{uL}	Turbulent length scale (m)
T_u	Turbulent intensity factor (%)
u	Mean flow velocity (ms^{-1})
$\mathbf{v}$	Velocity vector (ms^{-1})
W	Width of the channel (m)
x, y, z	Cartesian coordinates (–)
y^+	Non dimensional measurement of distance from a wall (–)
y	normal distance from the wall to the wall-cell centroid (m)
$u^\star$	reference velocity (m/s)

Greek Symbols

α	Attach angle (°)
α_D	Thermal diffusivity (m^2s^{-1})
β	Roll angle (°)
λ	Thermal conductivity ($Wm^{-1}K^{-1}$)
ϵ	Rate of dissipation (-)
$\gamma_{1,2}$	Base angles (°)
ρ	Density (kgm^{-3})
μ	Dynamic viscosity (Pas)
ν	Kinematic viscosity (m^2s^{-1})
∇	Mathematical operator stands for partial derivative (–)
ω	Stream-wise vorticity and specific turbulence dissipation rate (–)
Ω	Vorticity flux (–)

Subscript

t	Turbulent
in	Inlet parameters
out	Outlet parameters
w	Wall
x	Variable Cartesian coordinate
0	Empty channel parameters

Several designs and shapes of VGs are investigated through varying the application and the flow conditions. These investigations can either be made through experimental or numerical studies. Dogan and Igci [14], experimentally compared the delta winglet VG design against novel type vortex generator (NTVG) in a rectangular channel using stereoscopic PIV. The results showed that the heat transfer was enhanced by 34%.

Fu et al. [15] studied the configuration effects of the delta winglet longitudinal vortex generators and channel height on flow and heat transfer in mini-channels. The common-flow-down (CFD) and common-flow-up (CFU) configurations are considered in addition to different arrangement on the opposite walls which leads are five total configurations. Also, four channel heights (1, 2, 4 and 8 mm) are considered cover a wide channel aspect ratio (0.125–1). Reynolds number varies from 3000 to 18,000. Results showed that the mixed configuration (CFD and CFU) at $H = 1$ mm and the CFU1 configuration at $H = 2$ mm achieved the best heat transfer enhancement performance where their Nusselt numbers are increased by 28–35% and 27%–33% respectively, compared with smooth channels. Moreover, various VG designs are used and studied in the literature such as circular slice shaped VG's [16], curved winglet VGs with or without punched holes [17], helical and twisted VG [18], wavy fin and oval-tube bank with mounted VGs [19,20], composite fin with VGs [21], and longitudinal vorticity [22].

Increasing the Reynolds number to high values results in reaching turbulent flows. Thus, several models can be used to model the turbulence in channel flows. Behfard and Sohankar [23] studied the flow structure dynamics for a flow with Delta Winglet Pair (DWP) in a finned circular heat exchanger using a steady SST $k-\epsilon$ turbulence model. The results showed that convective heat transfer ratio and thermal performance factor approximately increase by 59% and 43%, respectively. Demirag et al. [24] investigated experimentally and numerically a novel type conic vortex generator (NTCVGs) in solar air heater fitted on the absorber plate with variable Reynolds number (Re = 5000–25000). Turbulence is modeled using the Shear-Stress Transport (SST) $k-\omega$. The highest thermal enhancement factor ($TEF = 1.316$) is achieved at attack angle ($\alpha = 37.5°$), blade angle ($\beta = 30°$) and aspect ratio ($S = 1:1$), respectively. Oneissi et al. [25] studied the effect a novel VG design Inclined Projected Winglet Pair (IPWP) on the heat transfer enhancement (ζ) with turbulent flow using the SST $k-\omega$ model. It results in an increase of ζ by 30% at Reynolds number $Re = 4600$ with respect to the empty channel. Charbel et al. [26] studied the fluid flow, inside a channel with VGs experimentally and numerically, to test which numerical model best predicts the fluid flow with VGs. Results showed that the SST $k-\omega$ model is better than the RNG $k-\epsilon$ model for such fluid flow by comparing the data to Stereoscopic Particle Image Velocimetry (SPIV) experimental data.

In order to optimize VGs designs, various shape and parametric optimization techniques are performed. Shao et al. [27] performed a multi-objective optimization of a micro-channel heat sink combining cavities and longitudinal vortex generators based on CFD and NSGA-II genetic algorithm at low Reynolds number (Re) ranges from 150 to 325. It is found that the proposed design achieve the best thermal-hydraulic performance compared to simple designs of heat sinks. Khan and Li [28] used multi-objective optimization algorithm (MOA) with the apply of BRANN (Bayesian-regularized artificial neural network)

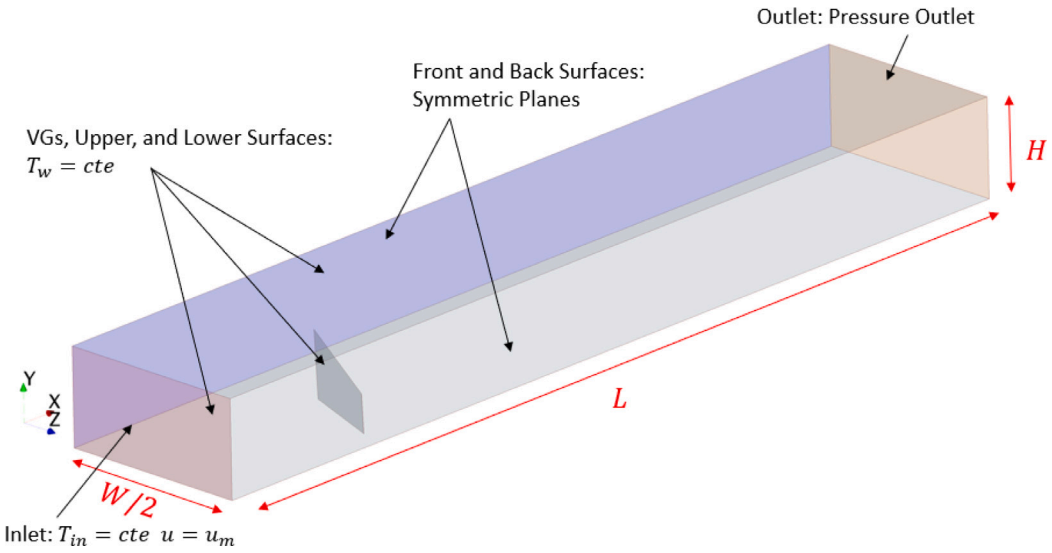

Fig. 1. Geometry and boundary conditions.

technique for obtaining an optimized vortex generator design. Yang et al. [29] performed an Response surface methodology (RSM) approach to optimize the thermal performance of a novel type vortex generators (NTVG). Results showed that the obtained optimum design has an increased thermal performance factor by 9.1% compared to smooth channel. Previously, Karkaba et al. [4] performed a multi-objective function optimization through large space exploration design to find optimal VG design with seven design variables with laminar flow. A new enhanced VG design was found with an increase of thermal enhancement factor by 35% and 14% relative to a smooth channel and better than literature results respectively.

Recently, many authors study the variation of VG forms but within a restricted VG shapes as triangular and rectangular shapes or even projections of these basic forms. Researchers performed wide parametric optimization studies on classical or basic VGs forms, but these studies were confined by varying one or two shape parameters like the VG angles (α, and β) regarding the flow direction. While results showed that VG performance is affected strongly by geometrical variations that should be investigated.

In this study, the objective is to shed light (i) on the optimal design of VGs and their dependence on the turbulence levels by varying Reynolds number values; (ii) on the effect of the geometrical parameters on the VG performance. For this reason, VG shape optimization is performed at different turbulent flow regimes by varying seven design parameters. The knowledge of the variation of the optimal shape of the vortex generator as a function of the flow regime is a crucial element for optimizing energy efficiency when sizing heat exchangers, micro-channel, solar heaters, etc. Thus, flow structure local analysis is carried out through highlighting the main difference of the obtained optimum VG design with classical VG shapes at different Re values. In addition, flow distribution and gradient variations are distinguished based on the VG shape and orientation depending on the flow intensity level. Pairs of VGs were considered with a common flow down (CFD) configuration as it is the most studied configuration due to its favorable physical behavior.

2. Computational fluid dynamics

2.1. Geometry, and boundary conditions

The computational design consists of a rectangular channel with the following dimensions height $H = 20$ mm, width $W = 4H$, and length $L = 10H$ as shown in Fig. 1.

The dimensions of the VG and the design parameters are shown in Fig. 2. Various shapes of the VG such as triangular, rectangular, and trapezoidal can be controlled by varying a parameter called shape length (SL) from [$SL = 0$ to $SL = h$] as shown in Fig. 2a. In addition following parameters are varied in the optimization study: VG height (h), length (l), and the base angles (γ_1 *and* γ_2) as shown in Fig. 2a.

On the lower surface of the channel, two VGs are inserted. Both are downstream the channel inlet by a distance ($s = 2H$). In addition, the distance ($d = 0.5H$) stands for the separation distance between VGs as shown in Fig. 2c. Symmetry was imposed at the middle of the channel ($W = \pm 2H$) as shown in Fig. 2b. Lastly, the most studied VG angle parameters through literature are also considered that are angle of attack α and the roll angle β that changes the flow direction that faces the VG.

In the present study, the boundary condition considered are as follows:

- Inlet: uniform velocity inlet u_{in} with an imposed constant temperature T_{in}.
- Upper and lower channel surfaces: a constant temperature T_w.
- VG surface: a constant temperature T_w.
- Left and right channel surfaces: a symmetric boundary condition.
- Outlet: a zero pressure value is applied for a Neumann boundary condition.

2.2. Governing equations

The flow field in the channel is three-dimensional and unsteady. The choice of the unsteady solver was due to the flow may exhibit a non-steady solution, transient solutions tend to be numerically more stable, and finally, the solution controls are too restrictive to converge a steady state solution. The fluid is treated to be incompressible having constant properties. The values of Reynolds numbers considered in the present study are $Re_1 = 4600$, $Re_2 = 9920$, and $Re_3 = 30050$.

The continuity (Eq. (1)), momentum (Eq. (2)), and total energy (Eq. (3)) are considered; governing equations are defined as the following:

$$\nabla.[\mathbf{v}] = 0 \tag{1}$$

$$\rho\frac{\partial}{\partial t}[\mathbf{v}] + \rho\nabla.[\mathbf{vv}] = -\nabla p + \nabla.(\mu + \mu_t)\left[\nabla\mathbf{v}\right] \tag{2}$$

$$\rho C_p\frac{\partial}{\partial t}[T] + \rho C_p\nabla.[\mathbf{v}T] = C_p\nabla.\left(\frac{\mu}{Pr} + \frac{\mu_t}{Pr_t}\right)\left[\nabla T\right] \tag{3}$$

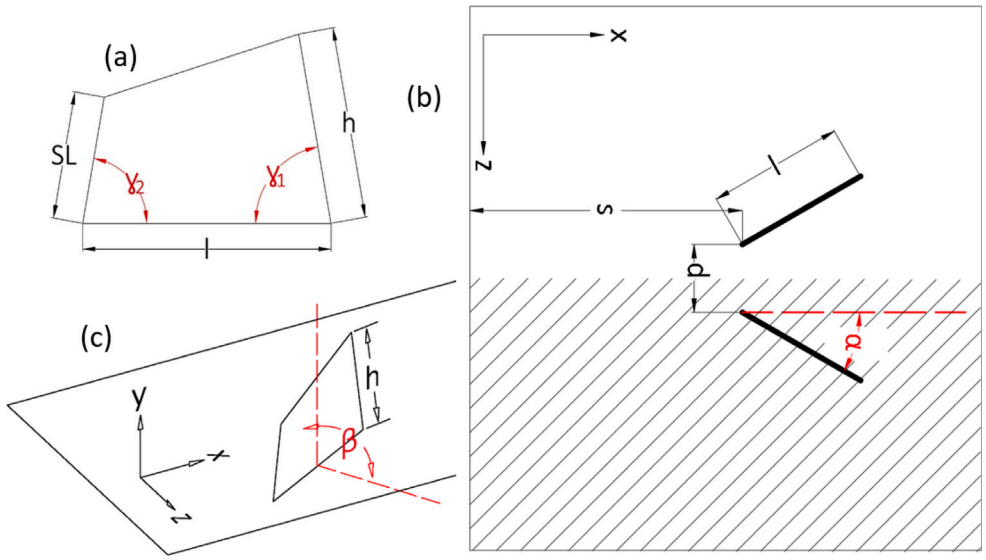

Fig. 2. Vortex generator dimensions (a), side view of VG (b), and top view of VG (c) inside the channel.

where **v** is the velocity vector, T is the temperature, ρ the fluid density, μ the fluid dynamic viscosity, μ_t is the turbulent viscosity, Cp the specific heat at constant pressure, ∇ is the gradient operator, and Pr_t is the turbulent Prandtl number.

The Shear-Stress Transport (SST) $k-\omega$ model developed by Menter [30] is employed for turbulent flow cases in the present contribution. This model adds two partial differential equations and then computes them. These equations are the modified version of the turbulence kinetic energy equation (k) and the transport equation for the specific dissipation rate (ω). The shear stress transport uses the $k-\omega$ formulation in the inner parts of the boundary layer and the $k-\epsilon$ formulation in the free stream. This model has an improved adverse pressure gradient performance compared to other models [26].

The modified version of $k-\omega$ turbulence model, (SST) $k-\omega$, that is employed for turbulent flow cases in the present contribution. is defined as follows [31]:

$$\frac{\partial}{\partial t}(\rho k)+\nabla.[\rho \mathbf{v} k]=\nabla.[\mu_{eff,k}\nabla k]+\overline{G}_k-Y_k \tag{4}$$

$$\frac{\partial}{\partial t}(\rho \omega)+\nabla.[\rho \mathbf{v} \omega]=\nabla.[\mu_{eff,\omega}\nabla \omega]+G_\omega-Y_\omega+D_\omega \tag{5}$$

where $\overline{G}_k$ is the production of turbulence kinetic energy due to mean velocity gradients, G_ω is the generation of ω, Y_k is the dissipation of k, Y_ω is the dissipation of ω, and D_ω is the cross-diffusion.

Air is used as a working fluid with the following properties: Prandtl number $Pr=0.708$, density $\rho=1.16\frac{\text{kg}}{\text{m}^3}$, thermal conductivity $k_f=0.02787\frac{\text{W}}{\text{m K}}$, dynamic viscosity $\mu=1.916\times10^{-5}$ Pa s, specific heat $Cp=1008\frac{\text{J}}{\text{kg K}}$. As for the turbulence properties, the turbulent intensity factor is $T_u=5\%$ usually taken as turbulence characteristic of the increasing airflow in such designs with a turbulent length scale: $T_{uL}=0.07D_h=2.8$ mm, with turbulent Prandtl number: $Pr_t=0.9$.

2.3. Numerical procedure and mesh sensitivity

The finite volume method is used in the present study to compute the governing equations using Star-CCM+ that is a computational fluid dynamics CFD software [32]. Pressure and velocity system of equations are solved in segregated manner. Momentum and continuity equations coupling were solved in a predictor–corrector approach. Second-order upwind scheme is used to discretize the convective terms in the momentum and energy equations. As for the diffusion terms, the second-order central scheme is applied. Velocity, pressure and temperature are solved via the algebraic multi-grid (AMG) linear solver with Gauss–Seidel relaxation scheme.

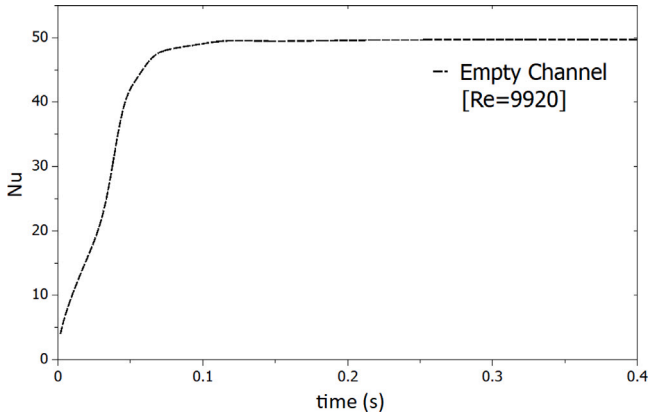

Fig. 3. Variation of Nusselt number (Nu) as function of the computational time in (s).

The convective terms defined for momentum, energy, and $k-\omega$ equations are discretized using a second-order upwind scheme. The dimensionless wall distance y^+ (Eq. (6)) refinement model is chosen in Star-CCM+ as a wall treatment for the turbulence model to ensure that the viscous sub-layer is meshed due to the adverse gradients beside the walls [32]. All governing equations are solved with implicit unsteady solver where the maximum physical time t computed from the formula $t=10\ L/u_{in}$ (domain length) with a time step $t_s=t/100$ and 15 inner iterations till reaching steadiness. Fig. 3 shows the variation of Nusselt number as function of the defined physical time at $Re=9920$. It is clearly observed that the value of the Nusselt number is stabilized after $t=0.2$ s for the defined case which ensures steadiness of the flow. Finally, for the convergence criterion, all the governing equations are solved iteratively until the residuals stabilized at below a small value 10^{-10} except for the energy and specific dissipation rate (SDR) residual below a value 10^{-6}.

$$y^+=\frac{yu^\star}{\nu} \tag{6}$$

where y is the normal distance from the wall to the wall-cell centroid, $u^\star$ is the reference velocity and ν is the kinematic viscosity.

Trimmed cells are used to generate a mesh in Star-CCM+ with a prism layer strategy that is applied near the walls in order to cover

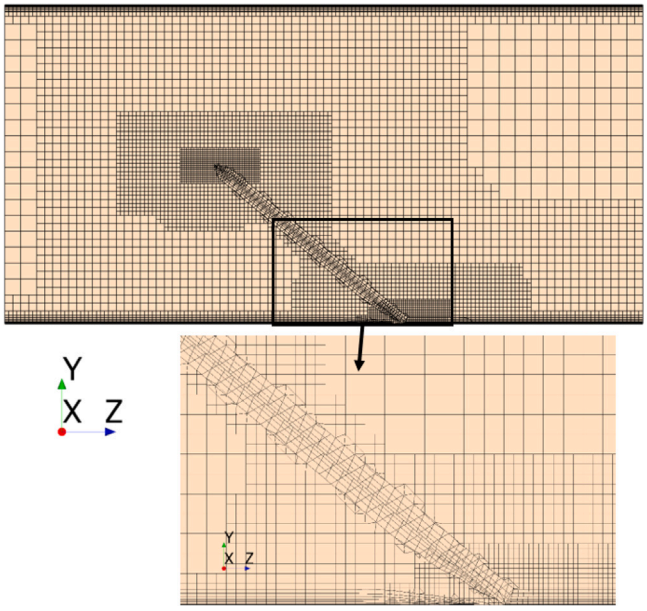

Fig. 4. 2*D* view of the mesh used in *y*–*z* direction at a vortex generator to show the refinement techniques used.

all the boundary layers. Two refinement methods (surface and curve refinements) found in Star-CCM+ are introduced to enhance the quality of the mesh especially at positions which exhibits larger variation gradients of velocity and temperature. Fig. 4 shows mesh generation with the refinement techniques beside the walls and downstream the VG. All the details for the mesh formation can be found our previous study Karkaba et al. [4].

The non-dimensional distance y^+ values for all of the design cases has a value smaller than 2 near the VG, and below 0.5 near the walls which are considered typical.

The grid convergence index (GCI) method is applied in order to precisely perform the mesh sensitivity analysis. The finally chosen mesh using this method contains 1.2×10^6 cells with less 2% GCI value [33]. The convergence of friction factor (f) and Nusselt number (Nu) as a function of the computational grid size is another approach that is applied for testing the selected mesh and is shown in Fig. 5. The mesh with 0.7×10^6 cells could have been selected if Nu has converged but there is still variation in f. Thus, the proposed mesh can be considered due to the stability of the two defined parameters that are clearly observed.

3. Results and discussion

3.1. Simulation validation

Before proceeding with the study, a validation for computational model is performed. A smooth square channel was considered where the turbulent models used in the present study are applied. Firstly, numerical results obtained from the present simulations are compared to a well known correlation result. Fig. 6(a) shows the Nusselt number Nu as function of Reynolds number Re for the present numerical study compared to Nu results computed from Dittus–Boelter Correlation [34]. As presented, the results shows a good agreement with minimum and maximum difference rates of 2% and 7% respectively taking into consideration that the Dittus–Boelter correlation fits best with ±20% uncertainty against their experimental data.

A second approach was adopted to validate the turbulence models used which is comparing the present results with experimental results. Tiggelbeck et al. [35] studied experimentally different types of VGs for heat transfer enhancement in channel flows. The delta winglet pair (DWP) VG design was chosen for the validation. Fig. 6(b) shows a comparison between numerical simulation and experimental results obtained by Tiggelbeck et al. [35]. The minimum and maximum error, between the experimental results and the present numerical results are 4.3% and 5.1% respectively taking into consideration that there is a ±10% uncertainty in the experimental results. There is an agreement between the results, which validates both the model and the method.

Table 1
Design parameters ranges.

Design parameter	Design interval	Increment value
α (°)	20:60	5
β (°)	20:80	5
γ_1 (°)	70:150	5
γ_2 (°)	110:170	5
h (mm)	10:19	1
SL (mm)	14:19	1
l (mm)	15:35	5

3.2. Optimization using a large space exploration design technique

In the present contribution, a large number of design parameters (seven parameters) are chosen to seek for optimal solutions using SHERPA method at different variation range for the design parameters and different turbulence levels depending on the value of Re. Systematic Hybrid Exploration, Robust, Progressive and Adaptive (SHERPA) is considered as a hyper-parameter optimization method that consists of a selection of strong dynamic algorithms [36]. In addition, it is robust, progressive and adaptive with a simultaneous hybrid exploration. It attempts firstly using multi search methods and records through selection the best attributes obtained for each search process. Thus leading to a reduction in the participating processes in seeking for the best one [37]. Thus, allowing to use stopping criteria for the processes with lower performances based on the criteria defined using the Median-Stopping-Rule [38]. The advantage of selecting SHERPA method is that it stands behind the fact that is a well adaptive optimization algorithm that varies the step size of the line-search process while progressing iteratively finding the optimal solution.

The set of parameters used each with its interval range variation used for all Re's are listed in Table 1.

The objective functions used for optimization are the friction factor f, Nusselt number Nu which, and thermal enhancement factor (ζ) also known as TEF which includes both Nu and f, are defined as follows:

$$f = \frac{p_{out} - p_{in}}{2\ \rho\ u_{in}^2}\ \frac{D_h}{L} \tag{7}$$

where p_{out} is the pressure value at the outlet, p_{in} at the inlet, and u_{in} is the uniform inlet velocity, and $D_h = 2(H \times W)/(H + W)$ is the hydraulic diameter.

$$Nu = \frac{hD_h}{\lambda} \tag{8}$$

where h is the local heat transfer coefficient, and λ the thermal conductivity.

$$\zeta = \left(\frac{Nu}{Nu_0}\right)\left(\frac{f}{f_0}\right)^{-1/3} \tag{9}$$

where the 0 subscript for Nu_0 and f_0 stands for the values of these parameters at an empty channel geometry.

For each case in the optimization study, a design interval for each parameter is defined as found in Table 1. The results obtained are then processed and analyzed to find the optimal design for each case with different Reynolds number ($Re_1 = 4600$, $Re_2 = 9920$, and $Re_3 = 30050$).

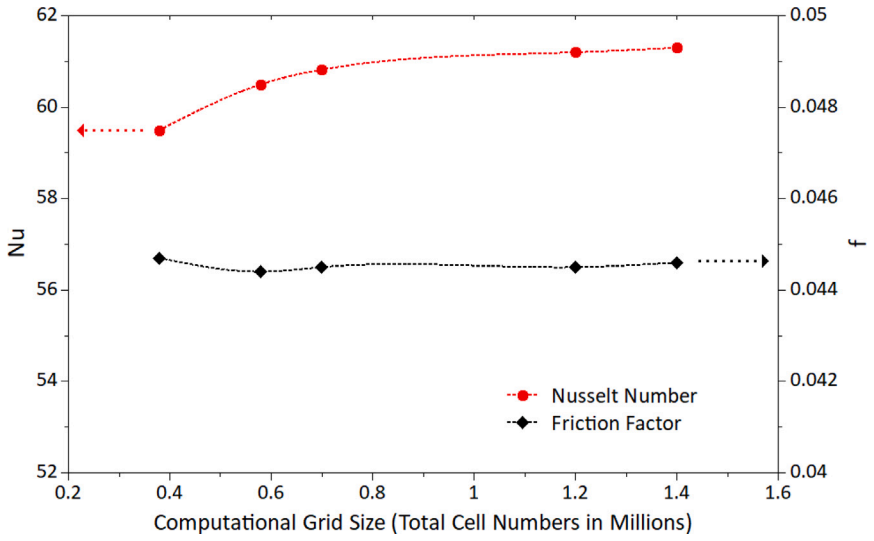

Fig. 5. Mesh sensitivity analysis variation of Nu and f as functions of computational grid sizes in millions.

Table 2
Fitting equation (10) constants for the Pareto Frontier at different Re.

Reynolds Number	Equation constants				
	a_0	a_1	a_2	a_3	a_4
4600	−4.278	158.4	−20,247	121,635	−273,196
9920	8.485	2,347	−37,503	288,968	−835,024
30050	63.58	2,590	−29,950	129,000	0

Table 3
Optimum design parameters values for the three Re studies.

Re –	α °	β °	γ_1 °	γ_2 °	h mm	SL mm	l mm
4600	35	50	75	150	19	19	30
9920	40	55	120	145	19	19	20
30050	30	70	130	140	17	19	20

Table 4
Global results for the three Re studies.

Re	ζ	Nu	Nu/Nu_0	f	f/f_0
4600	1.347	41.094	1.799	0.063	2.378
9920	1.239	61.089	1.677	0.044	2.480
30050	1.109	98.328	1.254	0.016	1.445

3.3. Pareto frontier

The obtained Pareto frontier results are shown in Fig. 7. It shows Nusselt number variation as function of the friction factor. It is clearly shown that the Pareto frontier curve is formed where a wide selection choice of optimal designs according to the two objective functions values (Nu and f). Although at each turbulent level and flow regime based on the values of Re, the design with the highest value of ζ is considered to be the optimum one. The optimum designs obtained denoted by $(*)$ symbol in each graph of Fig. 7 have the values of ζ = 1.347, 1.239, and 1.109 for $Re_1 = 4600, Re_2 = 9920$, and $Re_3 = 30050$ respectively. The optimum design (OD) for the study of $Re_1 = 4600$ is found after running 3360 designs with an overall time of 1984 h. The OD for $Re_2 = 9920$ is found after running 3092 designs and overall time of 1400 h. And the OD for $Re_3 = 30050$ is found after running 3755 designs and overall time of 1557 h. The simulations performed with a hardware of 32 logical processors.

The Pareto frontiers are found to fit well with polynomial law of fourth order (Eq. (10)) and for each Re the equation constants are given in Table 2:

$$Nu = a_0 + a_1 f + a_2 f^2 + a_3 f^3 + a_4 f^4 \tag{10}$$

The dimensions and shapes of the optimal designs ($*$ symbol of Fig. 7) are listed in Table 3 and shown in Fig. 8.

The values of the defined objective functions for the optimal designs are summarized in Table 4 for the three studies. The heat transfer enhancement is increased approximately through rounding by 35%, 24%, and 11% based on the thermal enhancement factor (ζ = 1.347, 1.239, and 1.109) with respect to the smooth channel geometry (empty channel) for the different Re ($Re_1 = 4600$, $Re_2 = 9920$, and $Re_3 = 30050$) respectively.

The results obtained for the optimization studies at different Re are compared to four results: classical well known vortex generators denoted as DWP and RWP, smooth channel computed in this present study and the IPWP design, i.e. inclined projected winglet pair vortex generators published by Oneissi et al. [25]. As mentioned, RWP and DWP VG designs are a well known and widely used in the literature studies presented in Chai and Tassou review [39] that have following geometric parameters $\alpha = 45°$, $\beta = 0°$, $\gamma_1 = 90°$, $\gamma_2 = 90°$, $l = H$, $h = 0.5H$, $SL = 0$ for DWP, and $SL = h$ for RWP as shown in Fig. 2. The present obtained results for the three studied cases are compared with the collected results from the literature and plotted as shown in Fig. 9. With 96% model accuracy, the heat transfer enhancement is increased for the present optimal design (OD) by 3.5%, 4.2%, and 14.4% with respect to the highest ζ value obtained previously by Oneissi et al. [25]. It should be also noticed that for the case with highest Reynolds number $Re = 30050$, for the present design that heat is enhanced while it is not, the in the other geometries which shows the good performance of the present design. These results clearly show the advantage of large exploration design that significantly enhanced VG performance at different flow regimes. In order to physically better understand the optimization results and the reasons of intensification mechanism, local investigation are now performed.

3.4. Qualitative local performance analysis

Flow structure and temperature distribution are analyzed, in order to better understand the heat transfer enhancement mechanisms when adding vortex generators.

Figs. 10, 11, and 12 show the velocity streamlines in addition to temperature distribution at different x/H locations through the channel. Upon adding VGs, an induced vortices are formed which mix and disturb the flow. In addition, the thermal boundary layer near

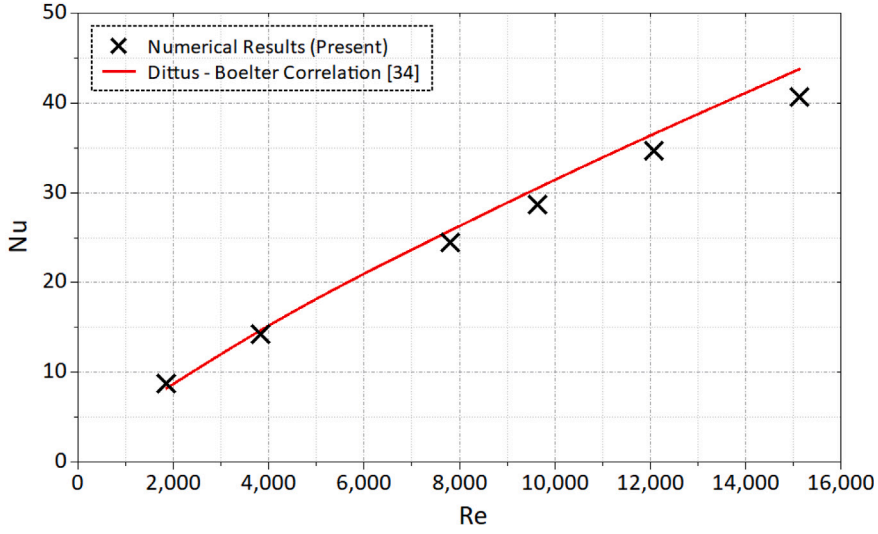

(a) Nusselt number Nu as function of Reynolds number Re for the present numerical results and correlated results obtained by Dittus-Boelter [34].

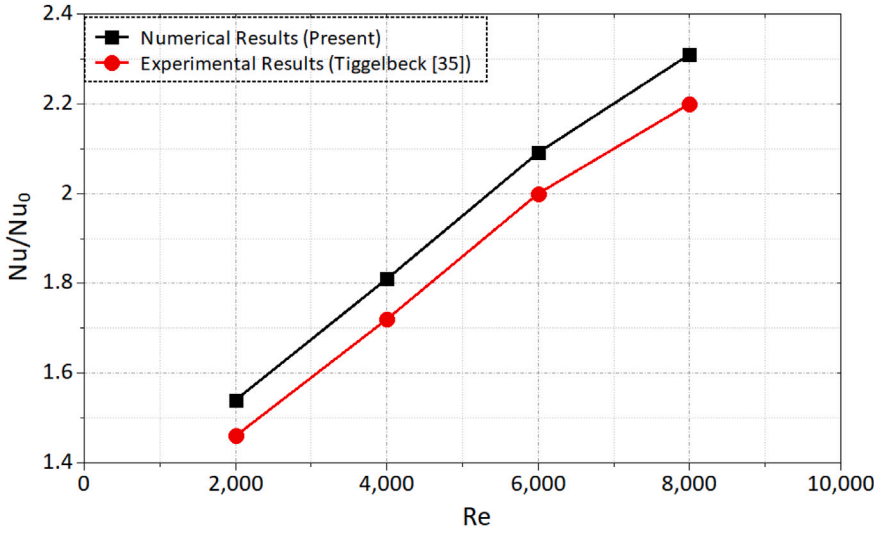

(b) Nusselt number Nu as function of Reynolds number Re for the present numerical results and experimental results obtained by Tiggelbeck *et al.* [35].

Fig. 6. Experimentally and numerically validation results.

the heated walls is broken which also increase mixing off the flow. Both of these two mechanisms will enhance the heat transfer inside the channel. And as shown in the figures, the vortices start to appear just at the upstream tip of the VG. It is clearly shown that the obtained shapes of VGs at turbulent levels, induce large vortices that affect the flow due to mixing and thus improve the heat transfer.

In Fig. 10 at $Re_1 = 4600$, an induced vortex (Vortex A) appears just at the upstream tip of the VG, then it starts to propagate downstream the channel. In addition, another vortex is formed (Vortex B) just at the lower tip of the VG beside the lower surface of the channel $z = W/2$ and $y = 0$. This generated vortex moves in the channel, downstream the VG and shifts gradually from $y = 0$ to approximately beside $y = H/2$. Vortices A and B has an influence on the heat transfer through enhancement due to their mixing effect. As for the temperature contours, it is clearly noticed that the thermal boundary layer at the heated walls is broken, that means the vortices disturb the development of the thermal boundary layers which improve the heat transfer beside the walls. In addition to the main vortices, it is observed that small vortices are induced inside the channel at different positions (corners of the channel), between the main vortices, symbolized by the symbol ⋆. Those vortices propagates along the channel until reaching its outlet. But they also indicate noticeable improvement effect on mixing. Although, these kind of vortices are previously studied and noticed in classical VG shapes where they are known as common flow down vortices. They create mixing effect between the VGs at the lower wall (down-wash) and above the VG (up-wash) at the upper wall of the channel. Due to the strong turbulence occurring inside the channel in various turbulence levels, the flow mixing is increased leading to enhanced heat transfer. For Figs. 11, and 12 with higher Re it is clearly observed the effect of the VGs shape on inducing vortices. That results in mixing the flow and increasing the heat transfer but with a weaker effect compared with lower Re (Fig. 10) due to VG shape and its lower turbulence level.

Another methodology used to analyze the vortices development is by tracking their formation at different successive locations. Thus to

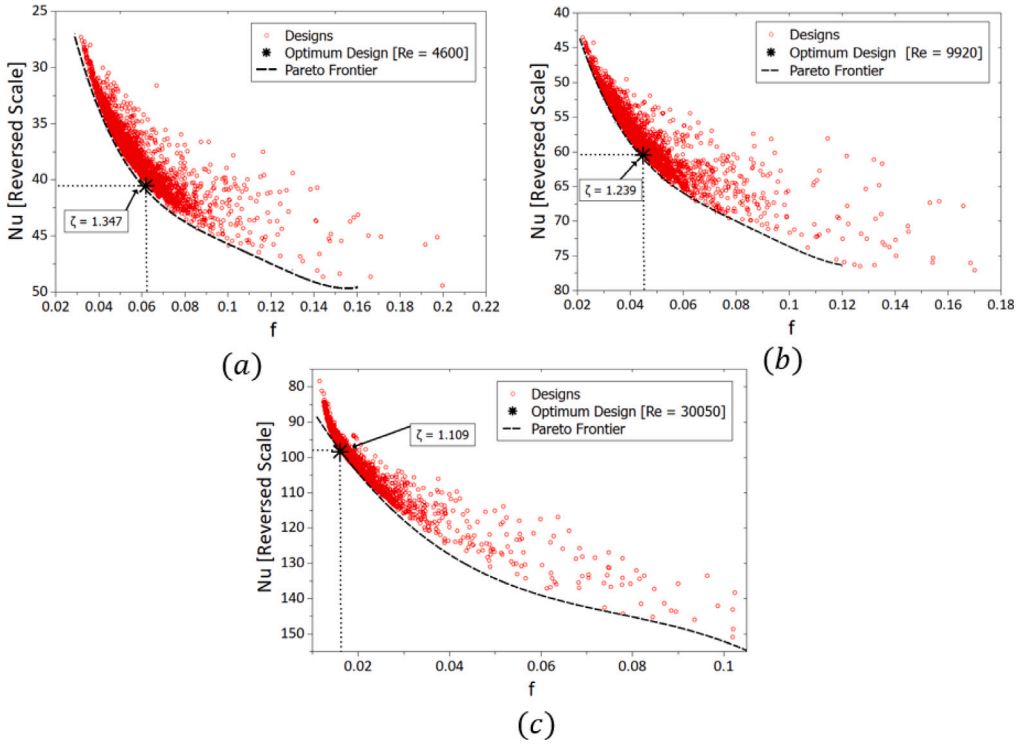

Fig. 7. Nusselt number variation as function of friction factor (a) $Re_1 = 4600$, (b) $Re_2 = 9920$, and (c) $Re_3 = 30050$.

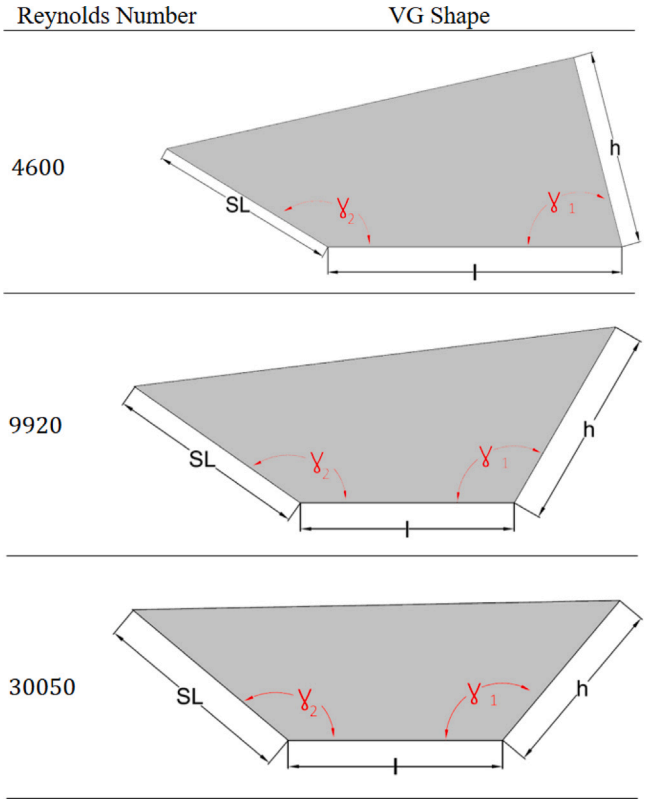

Fig. 8. Optimum design shape for the three Re studies.

do so, Lambda 2 (λ_2) criterion is considered that was proposed by Jeong and Hussain [40]. A vortex corresponds to a region where two eigenvalues of the symmetric part of the square of the velocity gradient are negative.

Fig. 13 shows the vortex cores detected by λ_2 criterion for the optimum designs. It is shown that upstream the VG at $x/H = 2$, where it is the formation beginning of the vortices, a very small red point appears inside the channel approximately at $z = W/4$ in the three cases. But, by comparing the three designs at $x/H = 4, 6$, and 8; the design at $Re_1 = 4600$ highlights the larger λ_2, that means a stronger turbulent flow disturbance. The vortex grows a lot while it moves downstream the channel mainly at the location of the large main vortex A, with a strong effect compared to other designs. While in the second case at $Re_2 = 9920$, the effect of the vortex core is smaller due to the weaker effect of turbulence with the higher Reynolds number value that decreases slightly the heat transfer rate by increasing the friction factor. This phenomenon can better be seen in the third case at $Re_3 = 30050$ where less vortical structure is induced compared to the other cases. It is concentrated around the main vortex due to the difference in VG designs that is according to angle β parameter value, that makes the VG more inclined with respect to the lower surface of the channel.

3.5. Quantitative local performance analysis

In addition to the qualitative analysis, another approach is used in order to locally quantify the performance of the various parameters as local bulk temperature, Nusselt number, friction factor, and vorticity flux. This analysis is performed for the obtained optimal designs by optimization and then compared to empty channel, and classical vortex generators (DWP and RWP) results. DWP and RWP designs as mentioned previously are well known shapes of VGs, their dimensions are as follows $\alpha = 45°$, $\beta = 0°$, $\gamma_1 = 90°$, $\gamma_2 = 90°$, $l = H$, $h = 0.5H$, $SL = 0$ for DWP, and $SL = h$ for RWP as shown in Fig. 2.

Firstly, the local bulk temperature T_b is computed and compared as mentioned with different VG designs for the three optimization studies

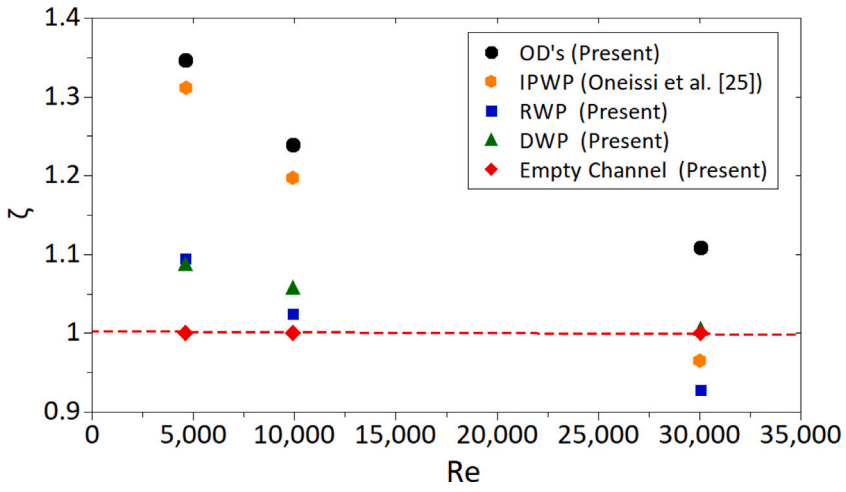

Fig. 9. Present and literature results for different Re [25].

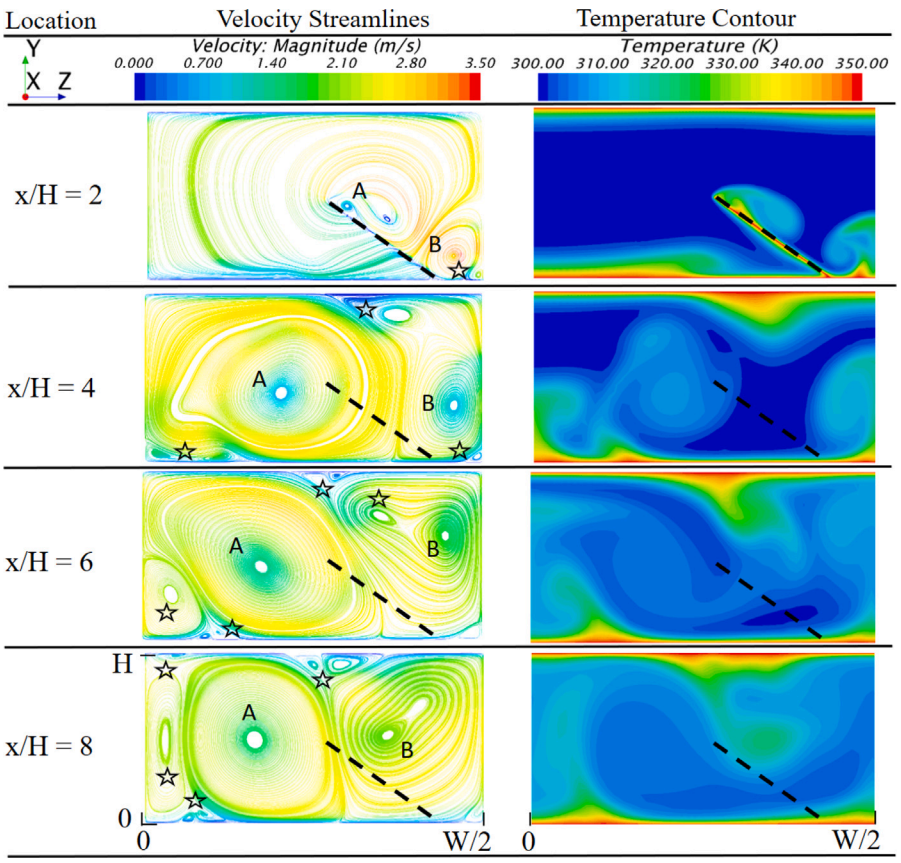

Fig. 10. Velocity streamlines and temperature distribution contours at different x/H locations (optimum design [$Re_1 = 4600$]).

and presented in Fig. 14. It is computed as a mass- flow averaged temperature at x/H traversal cross section along the passing of the flow through the channel. The variation of the local bulk temperature at $Re_1 = 4600$ is shown in Fig. 14(a). It should be noted that in the following presented figures, the dash-point and the point-point line styles represent the leading edge for optimum design and the other designs respectively. It is clearly shown that, upon reaching the leading edge of any VG, the temperature starts to increase compared to the smooth channel. For the present optimum design, the increase of the temperature is observed with a sharper slope with respect to the others and this is due to the shape of the VG and its higher mixing effect of the flow. In addition by observing the curves for the RWP and DWP, the temperature decreases just downstream the VG and then continue its increase through the channel. But for the present optimum design it starts increasing for at the leading edge of the VG and keep the same behavior until reaching the outlet. This higher increase of the temperature for the present design at $Re_1 = 4600$, leads to a better temperature increase at the channel end by 4.4 °C with respect to the highest temperature found for other design (RWP).

In Fig. 14(b), a variation of the local bulk temperature is observed at $Re_2 = 9920$ for the optimum design, RWP, DWP, and empty channel as function of x/H. The same profile is obtained: the present design provides a greater bulk temperature, but with a lower increase of the temperature at the channel end (2.5 °C) compared to the previous case.

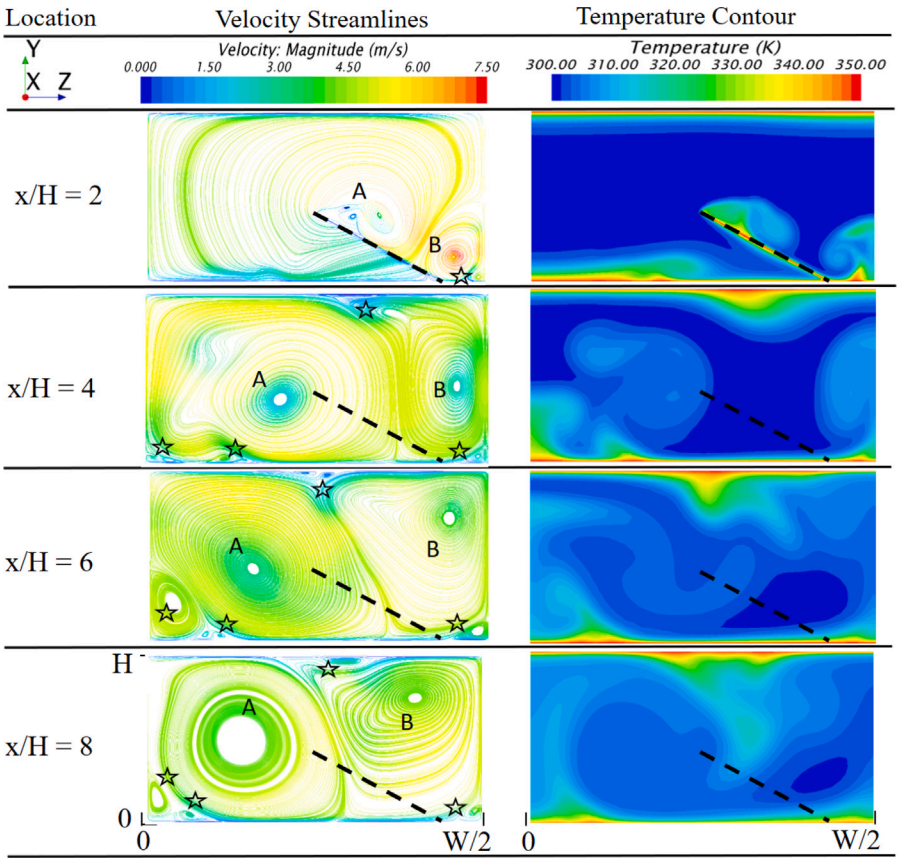

Fig. 11. Velocity streamlines and temperature distribution contours at different x/H locations (optimum design [$Re_2 = 9920$]).

In Fig. 14(c) at $Re_3 = 30050$, it is noticed that at the end of the channel there is no improvement with respect to the RWP design. Both the optimal design and RWP have approximately the same value of temperature. Thus, there is a need to seek and understand why ζ is enhanced in such design while the temperature remains the same.

For that reason, the local Nusselt number, defined in Eq. (11), is computed and presented in Figs. 15 as function of x/H locations.

$$Nu_x = \frac{h_x D_h}{k} \tag{11}$$

where

$$h_x = \frac{q''_x}{T_w - T_x} \tag{12}$$

and

$$T_x = \frac{\int u\, T\, dA}{\int u\, dA} \tag{13}$$

where q''_x is the boundary heat flux, T_x the temperature at each position, T_w the wall temperature, h_x the local heat transfer coefficient, Nu_x the local Nusselt number, k the thermal conductivity.

In Fig. 15(a) at $Re_1 = 4600$, the local Nusselt number variation for the present optimum design is much higher than the other designs and of course to the empty channel. For all designs, it exhibits a jump just at the leading edge of the VG. But for the optimum design, highest Nusselt number is observed from $x/H = 1$. In addition, Nu levels remain higher than other designs all over the channel and this is due to the strong effects of the vortices induced in such design. At $Re_2 = 9920$, similar conclusions can be drawn from Fig. 15(b).

In Fig. 15(c) at $Re_3 = 30050$, the local Nusselt number has a higher values compared to other designs just from $x/H = 1$ to $x/H = 2$, and then at $x/H = 2.5$ it remains the same as DWP and an obvious higher value is observed for the RWP case. In this case the heat transfer performance cannot be considered enhanced with respect to other designs, thus another parameters shall play the role in improving the overall heat transfer.

Another parameter that should be analyzed locally, is the local friction factor f_x that is defined in Eq. (14) and presented in Fig. 16. It is used to measure the pressure drop through the channel. It plays an important role in the pumping power throughout the channel. Thus maintaining an acceptable value for the friction factor is a critical key for improving the performance of the heat transfer. The friction factor is given by:

$$f_x = \frac{P_x - P_{in}}{\rho\, u^2}\ \frac{H}{L} \tag{14}$$

where P_x is the local pressure value at different cross sections, P_{in} is the inlet pressure, and u is the uniform inlet velocity.

Fig. 16(a) shows the variation of f_x as function of x/H at $Re_1 = 4600$. For the present study, f_x is found to be larger than the other designs. It is known that increasing the VG area affects the pressure drop due to the formation of stronger vortices but also strongly affects improvement of the heat transfer. As the new design of VG exhibits larger surface area, it is interesting to analyze the increase in f_x with the increase of surface area compared to ordinary designs. The area of the present optimum design is increased by a factor of 3.3 compared to RWP area while the friction factor is increased by 1.7. Comparing RWP VG design to DWP, the area is increased by a factor of 2 while the friction factor increases by 1.1. It is noticed that for this case, the increase of the area with the increase of friction factor is similar between each VG design and another. Thus it can be said that the present optimum design does not decrease the friction factor with respect to its larger surface area.

In Fig. 16(b) at $Re_2 = 9920$, it is clearly shown that the friction factor in the optimum design is lower than that of RWP for x/H between

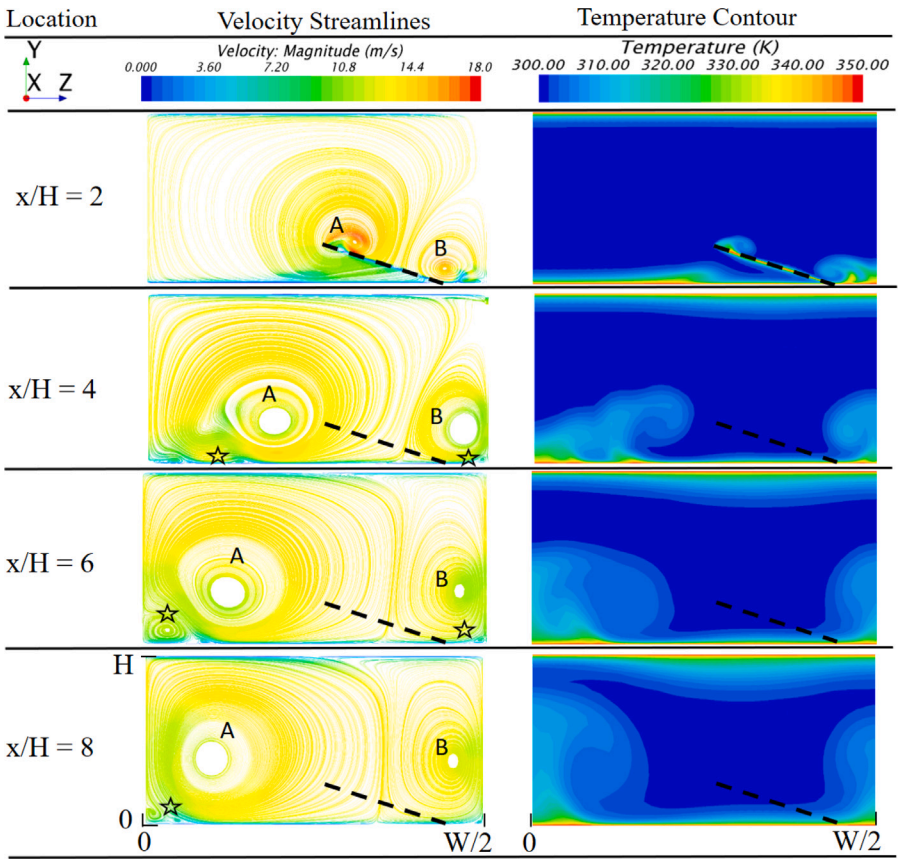

Fig. 12. Velocity streamlines and temperature distribution contours at different x/H locations (optimum design [$Re_3 = 30050$]).

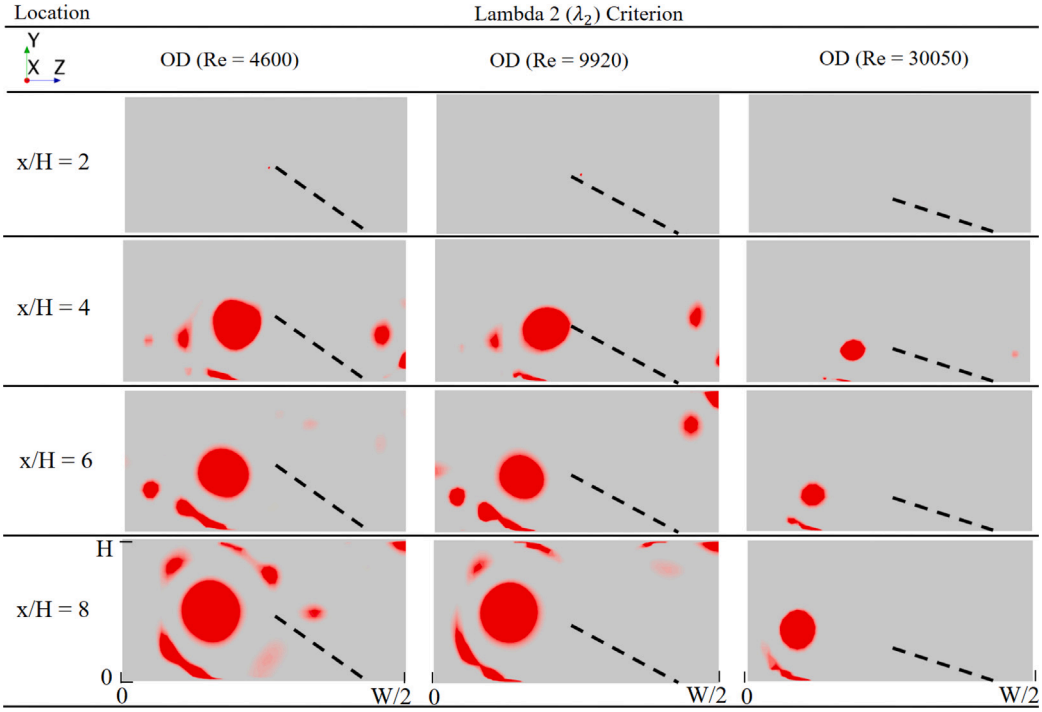

Fig. 13. Vortex core detected by λ_2 criterion for the optimum designs at $Re = 4600$, 9920, and 30050 respectively, at different x/H locations.

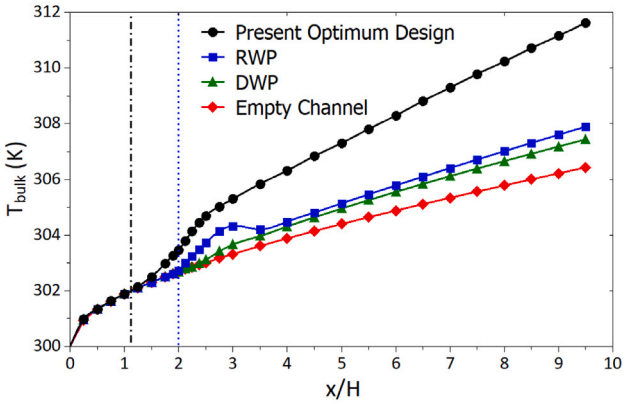

(a) Local bulk temperature T_b as function of different x/H locations at $Re_1 = 4600$.

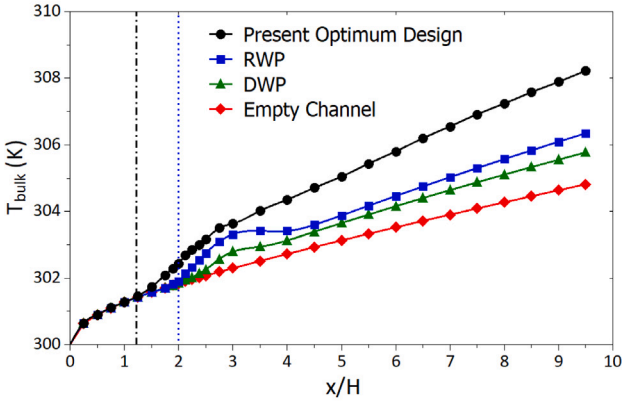

(b) Local bulk temperature T_b as function of different x/H locations at $Re_2 = 9920$.

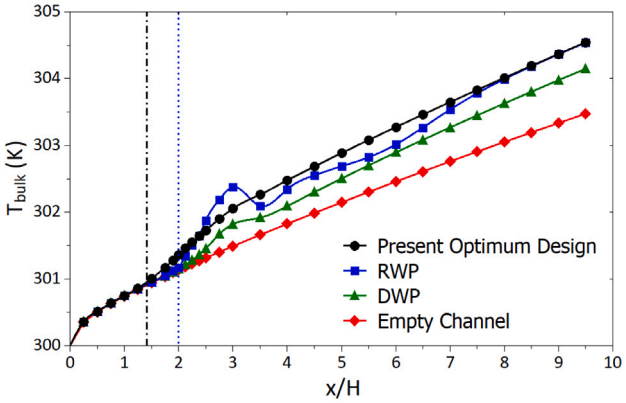

(c) Local bulk temperature T_b as function of different x/H locations at $Re_3 = 30050$.

Fig. 14. Local bulk temperature T_b as function of different x/H locations.

2.5 and 5, and higher than that of DWP. By studying the relation of increasing the area with the increase of the friction factor. The area of the present optimum design is increased by a factor of 2.7 compared to RWP and by 5.4 compared to DWP while the friction factor just increases by a factor 1.1 and 1.7, respectively. Thus, it can be concluded that for the present design, the surface area is increased but with a lower pressure drop compared to other classic designs. This can be explained by a contribution effect from the rolling angle β.

The optimum design at $Re_3 = 30050$ has the lowest friction factor, as shown in Fig. 16(c), compared to RWP and DWP (decrease by a factor of 0.5 and 0.8, respectively). While the area is increased by a factor of 2.85 and 5.7 compared to RWP and DWP, respectively. This can be explained by the high value of the rolling angle toward the lower surface, and its positive effect on the flow enhancement. As a conclusion, for high values of Reynolds number, it is more preferable to take into consideration the geometric parameters that can affect slightly the pressure drop in the domain, but also have an impact in enhancing the overall heat transfer.

3.6. Vorticity flux

The intensity of the secondary flow is used to quantify the effect of the longitudinal vortices [41]. Absolute spanwise-averaged streamwise vorticity flux j is used to examine the intensity effect and is computed

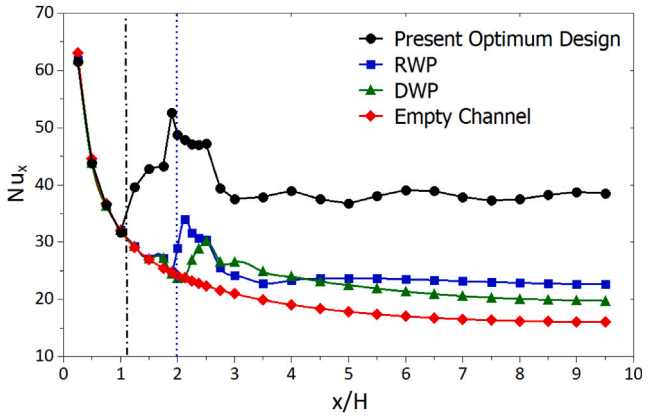

(a) Local Nusselt number Nu_x as function of x/H at $Re_3 = 30050$.

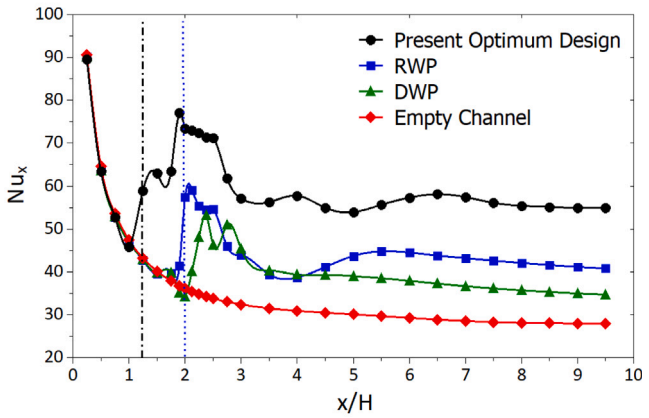

(b) Local Nusselt number Nu_x as function of x/H at $Re_2 = 9920$.

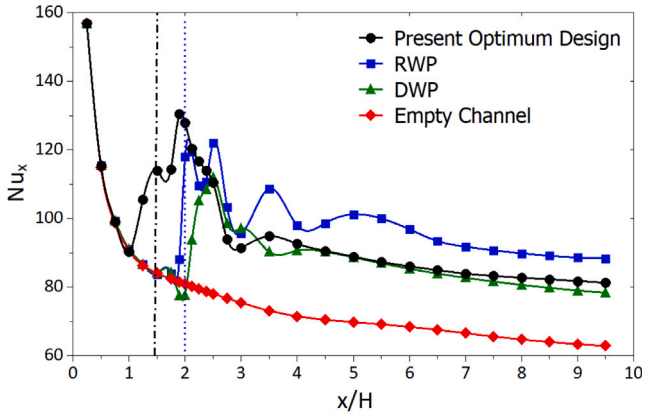

(c) Local Nusselt number Nu_x as function of x/H at $Re_3 = 30050$.

Fig. 15. Local Nusselt number Nu_x as function of different x/H locations.

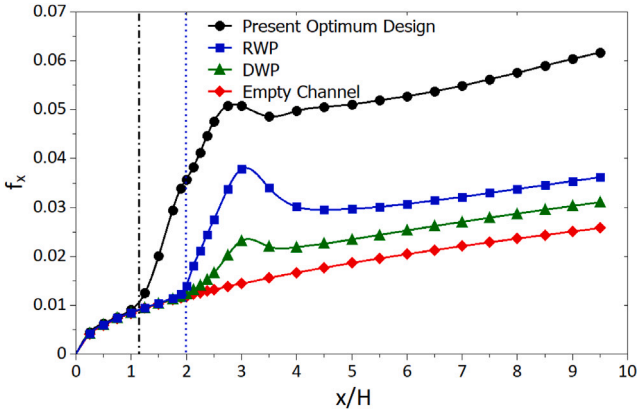

(a) Local friction factor f_x as function of x/H at $Re_1 = 4600$.

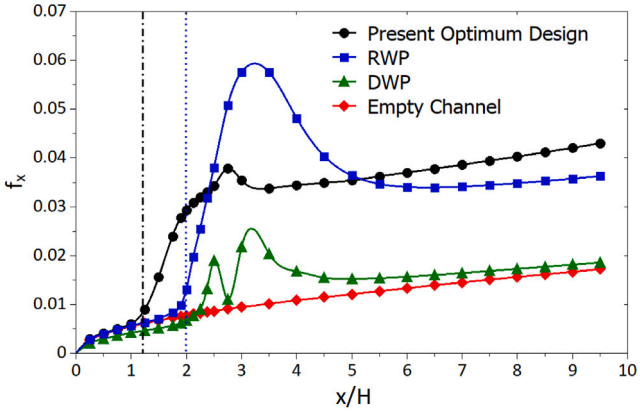

(b) Local friction factor f_x as function of x/H at $Re_2 = 9920$.

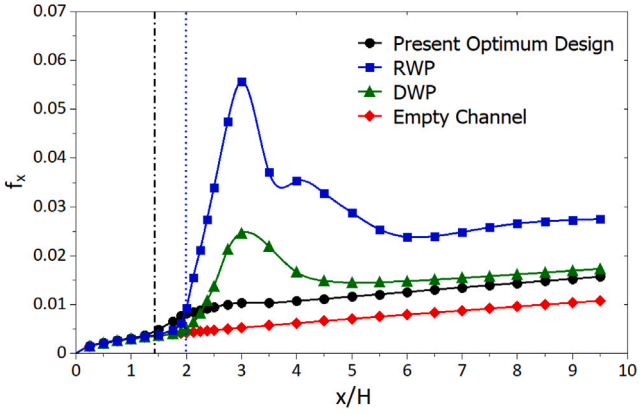

(c) Local friction factor f_x as function of x/H at $Re_3 = 30050$.

Fig. 16. Local friction factor f_x as function of different x/H locations.

as the following:

$$j = \frac{\int\int_S |\omega_x|\, dy\, dz}{\int\int_S dy\, dz} \tag{15}$$

where S is the channel cross sectional area, and ω_x is the streamwise vorticity. A dimensionless value of the absolute cross-averaged streamwise vorticity flux called hereafter vortices density, can be obtained from the following expression:

$$\Omega = \frac{j\ S}{u\ H} \tag{16}$$

where u is the mean flow velocity.

Figs. 17 shows the longitudinal evolution of the dimensionless vorticity flux at different Re ($Re_1 = 4600$, $Re_2 = 9920$, and $Re_3 = 30050$). In Fig. 17(a), a high value of Ω is observed for the obtained optimum design compared to the other designs. Ω of the obtained VG starts to increase rapidly when moving from the leading edge to reach the trailing edge of the VG. It then decreases slightly downstream the VG

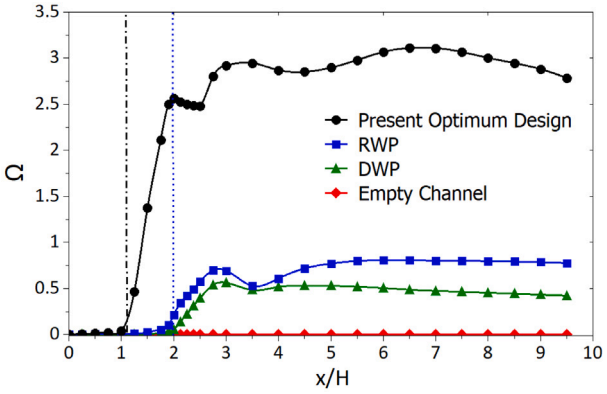

(a) Longitudinal evolution of the cross section-averaged vorticity flux as function x/H at $Re_1 = 4600$.

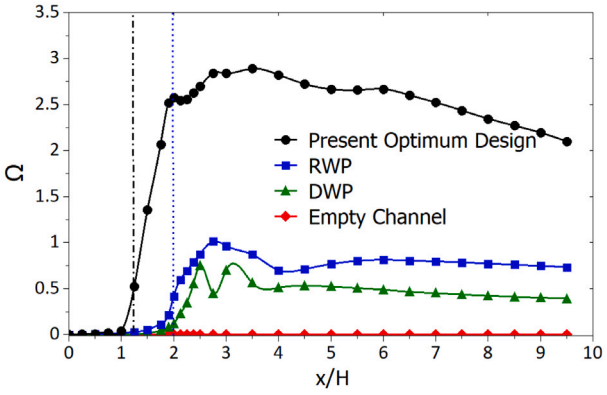

(b) Longitudinal evolution of the cross section-averaged vorticity flux as function x/H at $Re_2 = 9920$.

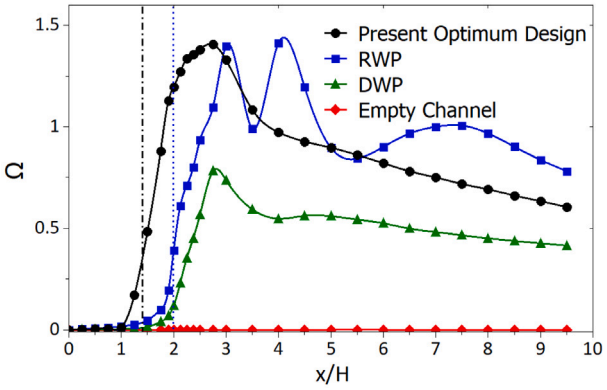

(c) Longitudinal evolution of the cross section-averaged vorticity flux as function x/H at $Re_3 = 30050$.

Fig. 17. Longitudinal evolution of the cross section-averaged vorticity flux as function of different x/H locations.

and then increases to a fluctuating value between 2.75 and 3 until reaching the end of the channel. Ω of the optimal design has larger values compared to other designs all along x/H.

Similarly, in Fig. 17(b) at $Re_2 = 9920$, a high value of Ω is observed for the obtained optimum design. It remains constant for a short distance then it increases slightly until it reaches the maximum value of $\Omega \simeq 2.8$ at $x/H = 3.5$ downstream the VG. Then it decreases slowly until reaching the end of the channel.

In Fig. 17(c) at $Re_3 = 30050$, the vorticity flux Ω is approximately the same compared to RWP, but higher compared to DWP. At the leading edge of the obtained optimal design, the vorticity flux is higher than that of the RWP due to the geometric difference in the position of the starting of the leading edge of the VG. It remains higher till reaching $x/H = 3.5$ where Ω, for the optimal design, keep decreasing. For RWP, it fluctuates between locations $x/H = 3$ and $x/H = 7.5$ until it decreases toward the end of the channel. It is noticed that Ω is higher compared to DWP, but is approximately the same for RWP.

3.7. Heat transfer performance analysis

A final interesting method is introduced in order to compare the present obtained designs with respect to other designs at different Reynolds numbers. This method was proposed by LaHaye et al. [42] that compute two dimensionless groups called the heat transfer performance factor J, and the pumping power factor F (Eqs. (17) and (18), respectively). These dimensionless numbers were used to quantify the performance of the heat exchangers. This method is used to plot all the

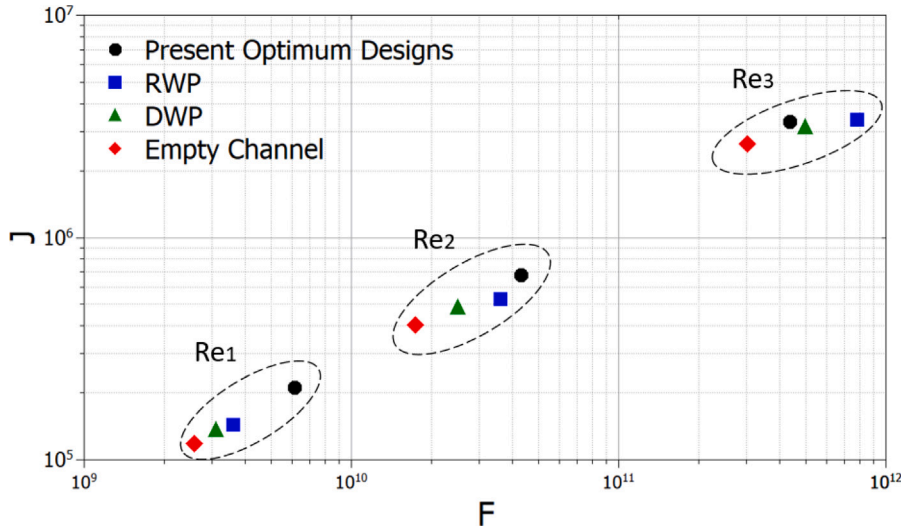

Fig. 18. Comparison of the heat transfer performance J versus pumping factor power F at different Reynolds numbers ($Re_1 = 4600$, $Re_2 = 9920$, and $Re_3 = 30050$).

designs at various Re on same graph for better understanding (for more details see [43]).

$$J = Nu\ Re\ Pr^{-1/3} \tag{17}$$

$$F = f\ Re^3 \tag{18}$$

where Pr is the Prandtl number.

Fig. 18 shows the variation of the heat transfer performance J versus the pumping power factor F of the optimum designs obtained at different Reynolds numbers ($Re_1 = 4600$, $Re_2 = 9920$, and $Re_3 = 30050$) compared to RWP, DWP, and empty channel. The comparison between the present VG designs and the other designs exhibits a higher pumping power factor F at same J and vice-verse.

4. Conclusion

In this study, a multi-objective function optimization is performed through large space exploration design to find optimal VG designs shapes. The numerical simulations are conducted inside a rectangular parallel plate channel under forced convection with different turbulence levels based on Reynolds number variation at ($Re_1 = 4600$, $Re_2 = 9920$, and $Re_3 = 30050$). A novel enhanced optimal VGs designs are found at each different Reynolds number which are different than the one found in the laminar optimization study performed previously by Karkaba et al. [4]. These designs are then compared to previous VGs from the open literature.

Optimization results indicate new enhanced VGs at different turbulent levels (low, medium and high) as follows:

- Low Turbulence at ($Re = 4600$): Thermal enhancement factor increased by 35%, and 3% relative to a smooth channel, and literature VG shapes respectively.
- Medium Turbulence at ($Re = 9920$): Thermal enhancement factor increased by 24%, and 4% relative to a smooth channel, and literature VG shapes respectively.
- High Turbulence at ($Re = 30050$): Thermal enhancement factor increase by 11%, and 14% relative to a smooth channel, and literature VG shapes respectively.

This shows that when the large number of parameters are considered in the optimization study, that means the degrees of freedom increase, it will lead to obtaining novel designs with better performance. Flow analysis and temperature distributions analysis are carried out in order to better understand the physical phenomena behind the heat transfer enhancement. It is observed that the obtained novel designs induce in the flow more vortices due to their geometric shapes that increase the mixing with the homogeneity of the temperature leading to increase the overall heat transfer enhancement.

Finally, local analysis is conducted that study the bulk temperature, Nusselt number, pressure loss (friction factor), and a normalized vorticity strength. The obtained results confirmed the understanding of the physical phenomena behind the enhancement and why the novel designs are considered better due to the effect of higher heat transfer while maintaining a similar friction factor values in cases with high Reynolds number.

The present work is carried out under forced turbulent convection. For future studies, other convection regimes with different flow regimes will be studied in order to observe if novel optimal designs can be found in each region.

CRediT authorship contribution statement

H. Karkaba: Writing – review & editing, Writing – original draft, Visualization, Software, Methodology, Conceptualization. **T. Dbouk:** Writing – review & editing, Validation, Supervision, Software, Methodology, Conceptualization. **C. Habchi:** Writing – review & editing, Validation, Supervision, Methodology, Investigation, Conceptualization. **S. Russeil:** Writing – review & editing, Validation, Supervision, Software, Project administration, Conceptualization. **T. Lemenand:** Writing – review & editing, Visualization, Supervision, Resources, Project administration, Conceptualization. **D. Bougeard:** Writing – review & editing, Supervision, Resources, Project administration, Funding acquisition, Formal analysis.

Declaration of competing interest

The authors declare that they have no known competing financial interests or personal relationships that could have appeared to influence the work reported in this paper.

Data availability

Data will be made available on request.

References

[1] P. Saini, A. Dhar, S. Powar, Performance enhancement of fin and tube heat exchanger employing curved delta winglet vortex generator with circular punched holes, Int. J. Thermofluids (ISSN: 2666-2027) 20 (2023) 100452, http://dx.doi.org/10.1016/j.ijft.2023.100452.

[2] S. Ali, C. Habchi, H. Zaytoun, M. Khaled, T. Dbouk, Surrogate-based optimization of the attack and inclination angles of a delta winglet pair vortex generator in turbulent channel flow, Int. J. Thermofluids (ISSN: 2666-2027) 20 (2023) 100473, http://dx.doi.org/10.1016/j.ijft.2023.100473.

[3] R. Aridi, S. Ali, T. Lemenand, J. Faraj, M. Khaled, CFD analysis on the spatial effect of vortex generators in concentric tube heat exchangers – a comparative study, Int. J. Thermofluids (ISSN: 2666-2027) (2022) 100247.

[4] H. Karkaba, T. Dbouk, C. Habchi, S. Russeil, T. Lemenand, D. Bougeard, Multi objective optimization of vortex generators for heat transfer enhancement using large design space exploration, Chem. Eng. Process. - Process Intensif. 154 (2020) 107982.

[5] M. Fahad, N. Ifraj, S. Tahsin, Md. Jahid Hasan, Numerical investigation of the hydrothermal performance of novel vortex generators in a rectangular channel by employing inclination and rotational angles, Int. J. Thermofluids (ISSN: 2666-2027) 20 (2023) 100500, http://dx.doi.org/10.1016/j.ijft.2023.100500.

[6] H. Karkaba, S. Russeil, J.V. Simo Tala, D. Bougeard, J. Boonaert, L. Etienne, U. Pelay, S. Lecoeuche, Effect of using multiple vortex generator rows on heat transfer enhancement inside an asymmetrically heated rectangular channel, Appl. Therm. Eng. (ISSN: 1359-4311) 227 (2023) 120359, http://dx.doi.org/10.1016/j.applthermaleng.2023.120359.

[7] S. Ali, S. Menanteau, C. Habchi, T. Lemenand, J.L. Harion, Heat transfer and mixing enhancement by using multiple freely oscillating flexible vortex generators, Appl. Therm. Eng. 105 (2015) 276–289.

[8] S. Ali, C. Habchi, S. Menanteau, T. Lemenand, J.L. Harion, Three-dimensional numerical study of heat transfer and mixing enhancement in a circular pipe using self-sustained oscillating flexible vorticity generators, Chem. Eng. Sci. 162 (2017) 152–174.

[9] C. Wang, Q. Lu, Y. Liu, H. Huang, J. Sun, Progressive review of heat transfer enhancement technologies in 2010–2020, Sustain. Energy Technol. Assess. (ISSN: 2213-1388) 56 (2023) 103121, http://dx.doi.org/10.1016/j.seta.2023.103121.

[10] Z. Brodnianská, S. Kotšmíd, Heat transfer enhancement in the novel wavy shaped heat exchanger channel with cylindrical vortex generators, Appl. Therm. Eng. (ISSN: 1359-4311) 220 (2023) 119720, http://dx.doi.org/10.1016/j.applthermaleng.2022.119720.

[11] H. Karkaba, L. Etienne, U. Pelay, S. Russeil, J. Simo tala, J. Boonaert, S. Lecoeuche, D. Bougeard, Performance improvement of air cooled photo-voltaic thermal panel using economic model predictive control and vortex generators, Renew. Energy (ISSN: 0960-1481) 218 (2023) 119332, http://dx.doi.org/10.1016/j.renene.2023.119332.

[12] S. Chamoli, R. Lu, D. Xu, P. Yu, Thermal performance improvement of a solar air heater fitted with winglet vortex generator, Sol. Energy 159 (2018) 966–983.

[13] J. Ye, Z. Peng, G. Tan, Multivariable analysis of vortex generator-aided heat transfer enhancement for 18650 battery thermal management system, J. Energy Storage (ISSN: 2352-152X) 82 (2024) 110516, http://dx.doi.org/10.1016/j.est.2024.110516.

[14] M. Dogan, A. Igci, An experimental comparison of delta winglet and novel type vortex generators for heat transfer enhancement in a rectangular channel and flow visualization with stereoscopic PIV, Int. J. Heat Mass Transfer 164 (2021).

[15] Hao Fu, Haiou Sun, Lianfeng Yang, Lanyi Yan, Yigang Luan, Franco Magagnato, Effects of the configuration of the delta winglet longitudinal vortex generators and channel height on flow and heat transfer in minichannels, Appl. Therm. Eng. (ISSN: 1359-4311) 227 (2023) 120401, http://dx.doi.org/10.1016/j.applthermaleng.2023.120401.

[16] A.U. Tepe, H. Yilmaz, Thermal–hydraulic performance of the circular-slice-shaped-winglet for tube bank heat exchanger, Int. J. Therm. Sci. (ISSN: 1290-0729) 179 (2022) 107711, http://dx.doi.org/10.1016/j.ijthermalsci.2022.107711.

[17] L. Zhao, Z. Qian, X. Wang, Q. Wang, C. Li, Z. Zhang, Analysis of the thermal improvement of plate fin-tube heat exchanger with straight and curved rectangular winglet vortex generators, Case Stud. Therm. Eng. (ISSN: 2214-157X) 51 (2023) 103612, http://dx.doi.org/10.1016/j.csite.2023.103612.

[18] G.S. Dhumal, S.N. Havaldar, Enhancing heat transfer performance in a double tube heat exchanger: Experimental study with twisted and helical tapes, Case Stud. Therm. Eng. (ISSN: 2214-157X) 51 (2023) 103613, http://dx.doi.org/10.1016/j.csite.2023.103613.

[19] K. Song, D. Hu, Q. Zhang, K. Zhang, X. Wu, L. Wang, Thermal-hydraulic characteristic of a novel wavy fin-and-circle tube heat exchanger with concave curved vortex generators, Int. J. Heat Mass Transfer (ISSN: 0017-9310) 194 (2022) 123023, http://dx.doi.org/10.1016/j.ijheatmasstransfer.2022.123023.

[20] D. Hu, Q. Zhang, K. Song, C. Gao, K. Zhang, M. Su, L.B. Wang, Performance optimization of a wavy finned-tube heat exchanger with staggered curved vortex generators, Int. J. Therm. Sci. (ISSN: 1290-0729) 183 (2023) 107830, http://dx.doi.org/10.1016/j.ijthermalsci.2022.107830.

[21] X. Wu, W. Zhang, Q. Gou, Z. Luo, Y. Lu, Numerical simulation of heat transfer and fluid flow characteristics of composite fin, Int. J. Heat Mass Transfer (ISSN: 0017-9310) 75 (2014) 414–424.

[22] C. Habchi, J.L. Harion, S. Russeil, D. Bougeard, F. Hachem, A. Elmarakbi, Chaotic mixing by longitudinal vorticity, Chem. Eng. Sci. 104 (2013) 439–450.

[23] M. Behfard, A. Sohankar, Numerical investigation for finding the appropriate design parameters of a fin-and-tube heat exchanger with delta winglet vortex generators, Heat Mass Transf. 52 (2016) 21–37.

[24] H.Z. Demirag, M. Dogan, A.A. Igci, The experimental and numerical investigation of novel type conic vortex generator on heat transfer enhancement, Int. J. Therm. Sci. (ISSN: 1290-0729) 191 (2023) 108383, http://dx.doi.org/10.1016/j.ijthermalsci.2023.108383.

[25] M. Oneissi, C. Habchi, S. Russeil, D. Bougeard, T. Lemenand, Novel design of delta winglet pair vortex generator for heat transfer enhancement, Int. J. Therm. Sci. (2016).

[26] C. Habchi, M. Oneissi, S. Russeil, D. Bougeard, T. Lemenand, Comparison of eddy viscosity turbulence models and stereoscopic PIV measurements for a flow past rectangular-winglet pair vortex generator, Chem. Eng. Process. - Process Intensif. (ISSN: 0255-2701) 169 (2021) 108637, http://dx.doi.org/10.1016/j.cep.2021.108637.

[27] J.K. Shao, Y.P. Hao, Z.Y. Li, Multi-objective optimization of a microchannel heat sink combining cavities and longitudinal vortex generators based on CFD and NSGA-II genetic algorithm, Int. J. Heat Mass Transfer (ISSN: 0017-9310) 220 (2024) 125019, http://dx.doi.org/10.1016/j.ijheatmasstransfer.2023.125019.

[28] T. T. Khan, W. Li, Optimal configuration of vortex generator for heat transfer enhancement in a plate-fin channel, J. Therm. Sci. Eng. Appl. (2018).

[29] Z. Yang, J. Gu, X. Luo, Z. Qin, S. Zhou, P. Wang, W. Zhao, An RSM approach to optimize the thermal performance of novel type vortex generators, Prog. Nucl. Energy (ISSN: 0149-1970) 167 (2024) 104978, http://dx.doi.org/10.1016/j.pnucene.2023.104978.

[30] F.R. Menter, Two-equation eddy-viscosity turbulence models for engineering applications, AIAA J. 32 (8) (1994) 1598–1605.

[31] F. Moukalled, L. Mangani, M. Darwish, The finite method in computational fluid dynamics an advanced introduction with OpenFOAM and matlab, Fluid Mech. Appl. 113 (2015).

[32] Star-CCM+ User Manual, Wall Treatment Models Reference, [Accessed 6 July 2020].

[33] P.J. Roache, Quantification of uncertainty in computational fluid dynamics, Annu. Rev. Fluid Mech. 29 (1997) 123–160.

[34] F. Incropera, P.D. Dewitt, Introduction To Heat Transfer, fifth ed., John Wiley & Sons, 2006.

[35] St. Tiggelbeck, N.K. Mitra, M. Fiebig, Comparison of wing-type vortex generators for heat transfer enhancement in channel flows, ASME. J. Heat Transf. 116 (4) (1994) 880–885, http://dx.doi.org/10.1115/1.2911462.

[36] L. Hertel, J. Collado, P. Sadowski, P. Baldi, Sherpa: Hyperparameter optimization for machine learning models, in: 32nd Conference on Neural Information Processing Systems, NIPS, Montréal, Canada, 2018.

[37] Red Cedar Technology, SHERPA - An Efficient and Robust Optimization/Search Algorithm. WP-1023, Rev. 05.08. https://www.redcedartech.com/pdfs/SHERPA.pdf.

[38] D. Golovin, B. Solnik, S. Moitra, G. Kochanski, J. Karro, D. Sculley, Google vizier: A service for black-box optimization, in: Proceedings of the 23rd ACM SIGKDD International Conference on Knowledge Discovery and Data Mining, ACM, 2017, pp. 1487–1495.

[39] L. Chai, S.A. Tassou, A review of airside heat transfer augmentation with vortex generators on heat transfer surface, Energies 11 (2018) 2737.

[40] J. Jeong, F. Hussain, On the identification of a vortex, J. Fluid Mech. 285 (1) (1995) 69–94.

[41] T. Lemenand, C. Habchi, D.D. Valle, H. Peerhossaini, Vorticity and convective heat transfer downstream of a vortex generator, Int. J. Therm. Sci. 125 (2018) 342–349.

[42] P.G. LaHaye, F.J. Neugebauer, R.K. Sakhuja, A generalized prediction of heat transfer surfaces, Trans. ASME J. Heat Transf. 96 (1974) 511–517.

[43] K.M. Stone, Review of literature on heat transfer enhancement in compact heat exchangers, in: Air Conditioning and Refrigeration Center TR-105, Air Conditioning and Refrigeration Center, College of Engineering, University of Illinois at Urbana-Champaign, 1996.